Article:

Shi, J, Fan, H, Liu, X et al. (1 more author) (2014) Large Electrostrictive Strain in $(Bi_{0.5}Na_{0.5})TiO_3$-$BaTiO_3$-($Sr_{0.7}Bi_{0.2})TiO_3$ Solid Solutions. Journal of the American Ceramic Society, 97 (3). pp. 848-853. ISSN 0002-7820

https://doi.org/10.1111/jace.12712

Large Electrostrictive Strain in $(Bi_{0.5}Na_{0.5})TiO_3$–$BaTiO_3$–$(Sr_{0.7}Bi_{0.2})TiO_3$ Solid Solutions

Jing Shi,[‡] Huiqing Fan,[‡,†] Xiao Liu,[‡] and Andrew J. Bell[§]

[‡]State Key Laboratory of Solidification Processing, School of Materials Science and Engineering,

Northwestern Polytechnical University, Xi'an 710072, China

[§]Institute for Materials Research, School of Process, Environmental and Materials Engineering,

University of Leeds, Leeds LS2 9JT, United Kingdom

Abstract: Relaxor ferroelectrics, $(0.94\text{-}x)(Bi_{0.5}Na_{0.5})TiO_3\text{-}0.06BaTiO_3\text{-}x(Sr_{0.7}Bi_{0.2}\square_{0.1})TiO_3$ (BNT-BT-xSBT) ($0\leq x\leq 0.5$), were prepared by a solid state reaction process, and their structures were characterized by the transmission electron microscopy and Raman spectroscopy. The BNT-BT-0.3SBT has a very high electrostrictive strain S=0.152% with hysteresis-free behavior, much more than the reported S in other ferroelectrics. $S\sim P^2$ profiles perfectly follow the quadratic relation, which indicates a purely electrostrictive effect with a high electrostrictive coefficient (Q_{11}) of 0.0297 m^4C^{-2}. Even, its Q_{11} keeps at a high level in the temperature range from ambient temperature to 180 °C. The field-induced large electrostrictive strain of BNT-BT-0.3SBT was attributed to the existence of ferroelectric nanodomains.

[†] Corresponding author, E-mail: hqfan3@163.com, Tel: +86-29-88494463, Fax: +86-29-88492642

I. Introduction

Electromechanical actuators directly transform input electrical energy into mechanical energy. Of the many types of actuator materials including magnetostrictive, photostrictive, and shape memory alloys, piezoelectric and electrostrictive ceramics are widely used in applications requiring high generative force, high frequency operation, accurate displacement, quick response time, or small device size.[1] Electrostriction produces an expansion in the direction of the field regardless of its polarity, and this expansion relaxes back to zero when the field is removed. Electrostrictive materials can be categorized in a simplified version $S=Q*P^2$, where P, S and Q is polarization, strain and electrostrictive coefficients, respectively.[2] More commonly, this effect is utilized in lead-containing relaxor materials owing to their high level strain of 0.1% and Q value of $\sim 10^{-2}$ m^4C^{-2}.[3-6] However, making lead-free electrostrictive materials is highly desirable due to the increasing concern for environmental safety, since the lead compounds are toxic.

In relaxor ferroelectrics, the electrostrictive strain can be kept at a relatively high level in a wide temperature range due to the diffused phase transition.[1] Traditionally, the phase transition temperature of a relaxor ferroelectric at ambient temperature can enhance the electrostrictive property effectively. These days great interest has been devoted since complex dielectric behaviors with strong frequency dispersion and large electric field-induced strains were observed in (1-x)BNT-xBT based lead-free materials.[7-10] The origin of the observed large strain in these systems was identified as a consequence of a drastic reduction in the remanent strain due to the presence of a "non-polar" phase at zero field, which enables each unipolar cycle to fully utilize the inherently large poling strain of BNT-based materials.[11-13] Aksel et al.[14] and Ma et al.[15] demonstrated the large strain behavior is related with the nucleation of a mixture of nanodomains that disturbs the long-range ferroelectric order rather than a long-range phase transition. Schutz et al.[16] showed that the large strain response is a result of the breaking of Bi-O hybridization confirmed by in situ Raman spectroscopy. Recently lead-free $Bi_{0.5}Na_{0.5}TiO_3$-based solid solutions exhibit high electrocstrains with slight hysteresis.[17-21]

It was reported that, in BNT-SBT, the formula scheme “a ferroelectric relaxor+a ferroelectric” for solid solutions leads to a high purely electrostrictive strain.[17,22] To further improve the electrostrictive property, the $(Sr_{0.7}Bi_{0.2}\square_{0.1})TiO_3$ in lead-free BNT-BT ferroelectrics with pseudocubic crystal structure at RT is introduced, where $(Sr_{0.7}Bi_{0.2}\square0.1)TiO_3$ is reported as a new lead-free ferroelectric relaxor.[17,21,22] In $(Sr_{0.7}Bi_{0.2}\square_{0.1})TiO_3$ strontium vacancies (□) are created to balance the charge misfit due to the substitution of divalent Sr ions by trivalent Bi ions. The materials for $(0.94\text{-}x)(Bi_{0.5}Na_{0.5})TiO_3\text{-}0.06BaTiO_3\text{-}x(Sr_{0.7}Bi_{0.2}\square_{0.1})TiO_3$ ceramics exhibit a very high electrostrictive strain at room temperature with hysteresis-free behavior. The electrostrictive strain S is up to 0.152% at ~ 80 kV/cm at room temperature for the sample with x=0.3 and the calculated electrostrictive coefficient Q_{11} is 0.0297 m^4C^{-2}, about 1.7 times the value of the electrostrictive coefficient compared with traditional Pb-based electrostrictors. Meanwhile, this high electrostrictive coefficient keeps at a high level in the accessible temperature range from room temperature to 180 ^oC. The TEM and Raman revealed that the formation of nanodomains around room temperature at x=0.3 plays a key role in field-induced large electrostrictive strain.

II. Experimental

Ceramic powders were fabricated by the mixed oxide route from high-purity raw powders being $BaCO_3$ (99.0%), Bi_2O_3 (99.9%), TiO_2 (98%), $SrCO_3$ (99%) and Na_2CO_3 (99.8%). The powders were weighed and mixed by ball milling in isopropyl alcohol for 6 h. After drying, the mixtures were calcined in a covered alumina crucible at 850 ^{o}C for 4 h. The calcined powders were ball milled again for 4 h, then compacted into pellets of 12 mm in diameter at a pressure of 140 MPa and sintered in air at 1125-1200 ^{o}C for 4 h. The resulting pellets were polished to a final thickness of 1 mm for property investigations. Sliver electrodes were coated on both the polished surfaces and fired at 850 ^{o}C for 20 min for electric test.

Phase structure of the powders ground from the sintered samples was investigated by X-ray diffraction (XRD) (XRD-7000, Shimadzu, Kyoto, Japan) with Cu K_{α} radiation in 2θ range of 20-80^{o} at room temperature. The surface morphologies of the ceramics were observed using a scanning electron microscope (SEM; JSM-5610, JEOL, Tokyo, Japan). The dependence of the electric polarization (P) and the longitudinal strain (S) on an external electric field (E) were measured at 1 Hz using a ferroelectric test unit (TF-2000, aix-ACCT, Aachen, German) for 20 ^{o}C-160 ^{o}C (Temperature controller, aix-ACCT, Aachen, German). The dielectric properties were measured using a precision impedance analyzer (4294A, Agilent, CA, USA). Raman spectra were obtained with an instrument (LabRAM HR800, Horiba Jobin Yvon, Lyon, France) in a backward scattering geometry (the exciting source was the 514.5 nm line from an argon ion laser). For the Raman study, the sintered pellets were polished on one side using diamond paste and then cleaned thoroughly with acetone. The samples were subsequently annealed at 400 °C for 8 h to remove any residual surface stresses left after the polishing. The variable temperature Raman spectra of the ceramics were stabilized at the desired temperature for 5 min prior to the spectrum measurement. TEM specimens were prepared from the as-sintered pellets through standard procedures including grinding, cutting, dimpling and ion milling. The dimpled disks were annealed at 250 ^{o}C for 2 h to minimize the residual stresses before Ar-ion mill to electron transparency. Lattice images were obtained by using a transmission electron microscopy (TEM; Tecnai F30, FEI, Hillsboro, OR, USA) operated at 300 kV accelerating voltage.

III. Results and Discussion

The XRD analyses of the powders ground from sintered BNT-BT-xSBT ceramic samples with x=0-0.5 revealed a single perovskite structure without apparent secondary phases, as provided in Fig. 1. The pseudocubic structures for all the composition range were studied as no peak splitting other than $K_{\alpha1}$ and $K_{\alpha2}$ was detected, supporting the fact that there is no obvious long-range noncubic distortion. The inset shows the SEM micrographs of BNT-BT-0.3SBT ceramics. It can be noticed that the ceramics are dense and have uniform structure.

Ferroelectric hysteresis loops (polarization P versus electric field E) of the samples were measured at ambient temperature at 1 Hz plotted in Fig. 2(a). The polarization hysteresis loop of x=0 displays a well-saturated typical ferroelectric behavior with the maximum and remanent polarizations of 43 and 33 µC/cm^2, respectively. It is noted that the remanent polarization of 33 µC/cm^2 drops drastically down to 2.6 µC/cm^2 at a substitution of 10 mol% SBT. It implies that the ferroelectric order is disturbed with the addition of SBT, leaving a “non-polar” phase at zero electric field. Due to their comparable free energies, nonpolar phase can transforms reversibly into a ferroelectric phase by an external electric field. For the samples with x=0.3, only a very slim P~E profile is observed, which is slimmer than that of other lead-free or lead-containing electrostrictors.[17,18,20] The currently observed P~E loop can be due to a normal relaxor for BNT-BT-0.3SBT. The P~E profile is almost linear in the samples with x=0.5, indicating a paraelectric behavior.

Electric field driven strains (S) at ambient temperature are shown in Fig. 2(b). Typical butterfly-type strain loop, whose maximum strain level is 0.37% and negative strain is 0.012%, was observed for the samples x=0 with predominant ferroelectric behavior. In contrast, x=0.1, 0.3 and 0.5 show a drastic deviation from the typical ferroelectric behaviour. Notice that the negative strain closely related to the domain back switching during bipolar cycles was disappeared with x=0.1. For x=0.3 the S~E curves show almost hysteresis free with strain value in the range of 0.152% at ~80 kV/cm and a quadratic variation P^2 with E. This strain level is comparable with other lead-containing electrostrictors.[17,18,23] The composition with x=0.5 also shows a quadratic variation P^2 with E, while the strain level decreased drastically.

Electrostriction can be particularly large in the following situations: 1) ferroelectric materials just above their T_C, where an electric field can enforce the energetically unstable ferroelectric phase.[3] 2) The phase transition temperature of a relaxor ferroelectric is close to ambient temperature. Therefore, we adjust the composition and dopants in BNT-6BT based lead-free ferroelectrics to produce a relaxor phase which can be induced to the FE at ambient temperature, and produce prominent lead-free electrostrictors. Fig. 2(c) displays the plots of $S\sim P^2$ with the composition of x=0.1 and 0.3. Evidently, the $S\sim P^2$ curves for the composition with x=0.3 is linear whereas that of x=0.1 is slightly deviated from linear relationship. That means the sample with x=0.3 is a pure relaxor without any macrodomain. In the meantime, the sample with x=0.1 is a predominant relaxor with some distribution of macrodomain. The averaged electrostrictive coefficient (Q) for x=0.1 and x=0.3 are calculated to 0.0233 m^4C^{-2} and 0.0295 m^4C^{-2}, respectively. The Q values of our materials are notably larger than other lead-containing and lead free electrostrictor.[17,18,23,24]

The temperature dependence of P~E loops at ~60 kV/cm of x=0.3 are shown in Fig. 3(a). The inset of Fig. 3(a) shows the maximum polarization (P_{max}) of different temperature. The P_{max} changed from 19.5 μC/cm^2 to 16 μC/cm^2 in the temperature range of 30~180 °C. In addition, the dissipated energy, i.e., the area of the P~E curves, are determined to be 0.084×10^6 J/m^3 for x=0.3 at ambient temperature. This value is lower than that of other reported electrostrictive materials.[18] Fig. 3(b) displays the temperature dependence of S and Q_{11} curves at ~60 kV/cm which exhibit an excellent thermal stability. Q_{11} increases little, with variation less than 5% in the temperature range between 30~180 °C. It is noted that the S and Q_{11} remain high in a wide range from room temperature up to 180 °C and exhibit better thermal stability than other electrostrictors.

The temperature dependence of the relative dielectric permittivity (ε') and loss tangent ($\tan\delta$) for BNT-BT-xSBT samples (x=0, 0.1 0.3 and 0.5) are shown in Fig. 4. The inset shows $\Delta\varepsilon'$ (ε'_{1kHz}-ε'_{100kHz}, where ε'_{1kHz} is permittivity at 1 kHz and ε'_{100kHz} is permittivity at 100 kHz.) of samples with x=0-0.5 at ambient temperature. For all the samples two peaks are observed. One is the absolute maximum dielectric peak (T_m) without significant frequency dispersion, which is due to the "paraelectric-relaxor" phase transition. Another is a further, frequency dependent, anomaly of the permittivity at lower temperatures (T_{R-T}), with very pronounced frequency dispersion. Recently, it has been proposed in $0.94(Bi_{1/2}Na_{1/2})TiO_3$-$0.06BaTiO_3$ that T_m is related to a relaxation of tetragonal polar nanoregions (PNRs) emerged from rhombohedral PNRs, and T_{R-T} is ascribed to the thermal evolutions of discrete PNRs, which has nothing to do with any measurable structural transition.[25] With increasing SBT concentration, the T_{R-T} is shifted to a lower temperature compared with that of BNT-6BT and finally almost disappeared at x=0.5. In the meantime, the intensity of frequency dispersion increases, with $\Delta\varepsilon'$ increase from 260 for x=0 to 600 for x=0.3, which results in high permittivity at RT about 2323 compared with 1695 and

1431 of x=0 and 0.1, respectively. It is suggested that the cation disordering between A site is enhanced by increasing SBT and thus very intensive phase transition diffuseness, which were also found in other BNT-based solid solutions.[12,26,27]

Fig. 5 displays TEM micrographs and electron diffraction patterns from the same area in a grain with representative features for the composition x=0.1 and x=0.3. In Fig. 5(a), a grainy morphology is visible. Within the grains areas of 200 nm (marked with arrows) with lamellar domain contrast were frequently observed. Fig. 5(b) and 5(c) are the SAED patterns taken along the [100] and [110] zone axes, in which the 1/2 ooe in-phase and 1/2 ooo anti-phase (where “o” and “e” indicate an index with odd and even numbers, respectively) reflection are observed (marked by rings and arrows, respectively) besides the fundamental perovskite reflections. It has been noted that these superlattice reflections originate from slight deviations from the ideal perovskite structure, which could have intensity contributions from: (1) oxygen octahedral tilts; (2) chemical ordering of the A-site cations; and/or (3) antiparallel displacements of cations. In NBT, it is believed that oxygen octahedral tilting is the dominate source of the intensity.[28-31] These 1/2 ooe in-phase and 1/2 ooo anti-phase indicate the presence of the in-phase octahedral tilting ($a^{o}a^{o}c^{+}$) and antiphase octahedral tilting ($a^{-}a^{-}a^{-}$), which can be used to identify local rhombohedral (R) and tetragonal (T) phase regions. In Fig. 5(d), the grain contrast was homogeneous implying the presence of nanoscale features. The inset shows the larger version of nanodomains of x=0.3, which shows that the size of domain is 50 nm, and this is much smaller than that in the x=0.1 sample. Such observation has been reported in the TEM study of relaxor ceramics.[15,32-34] We observe that the intensity of the 1/2 ooo and 1/2 ooe of x=0.3 are weaker than that in the x=0.1. It suggests that the doped SBT destabilize the tetragonal and rhombohedral phase at room temperature, i.e. the structure is more cubic than other BNT-based materials.

The Raman spectra of BNT-BT-xSBT (x=0-0.3) from 50 to 1000 cm^{-1} at room temperature are shown in Fig. 6(a). The overall spectral signature demonstrates a relatively broad feature; which is in good agreement with previous reports.[35-38] This can be attributed to the A-site disorder and the overlapping of Raman modes due to the lattice anharmonicity. Raman spectra of BNT-BT-xSBT ceramics show most of the bands undergo constant shifting and broadening as the SBT concentration increases. Wavenumbers <≈200 cm^{-1} modes can be associated with vibrations of the perovskite A-site, thus involving Bi, Na, Ba and Sr cations. The mode at ≈125 cm^{-1} (marked by dotted arrow) has previously been assigned as belonging to A_1 symmetry and, more recently, associated with Na-O vibrations, and the other modes to vibrations involving the Bi-O bond (75 cm^{-1}).[21,39] With increasing SBT substitution, we observed an increase in FWHM of mode 75 cm^{-1} and a sudden drop in the wavenumber and intensity of mode at 125 cm^{-1}, which can be interpreted as a weakening of the A-O bonds. As a result of this change in the bond situation, a higher polarizability of the unit cells, resulting in the possible formation of nanodomains, which could be revealed in the TEM, is conceivable. A more-disordered lattice was obtained due to the presence of nanodomains produced by bond weakening (i.e., a more-cubic lattice). Conveniently, electrostrictive effects tend to be more pronounced in perovskites with a structure close to cubic, thus explaining the electrostrictive behavior of the material. In fact, the appearance of additional modes (marked by black arrow) in the spectral profiles gives an indication that the rhombohedral phase changes to cubic through an intermediate noncubic phase.[21] The mode at ≈260 cm^{-1} has been assigned as an A_1 mode closely related to the strength of the Ti-O bond. The splitting of this peak(s) (marked by red arrow) at room temperature with increasing SBT reveals a change in symmetry, to a structure whose irreducible representation has a higher number of Raman active modes. The mixed phase nature is signaled most clearly by the shoulders on both sides of the 260 cm^{-1} feature.[40,41] The high-frequency bands above 450 cm^{-1} have all been associated with TiO_6 vibrations, namely the breathing and stretching modes of the oxygen octahedra.

Variable-temperature Raman spectra (-160 °C-0 °C) in the range from 50 cm^{-1} to 1000 cm^{-1} are shown in Fig. 6(b). With increasing temperature, temperature-induced broadening occurs. The 260 cm^{-1} peak splitting persisted till -160 °C somewhat similar to that previously reported by Luo et al.,[37] which could also support the idea that higher structural disorder exists in the Ti-O bond of the TiO_6 octahedra with increasing temperature; such behavior may be associated with the nucleation of nanodomains within the ferroelectric matrix. The inset of Fig. 6(b) shows the details of the temperature dependence of the position of both the Bi-O and Ti-O modes. The softening of the Bi-O modes at -80 °C is due to a weakening of the Bi-O bonding by the increased thermal vibrations. Since the Ti-O bonds are influenced by the dynamics of the nanodomains phase,[42] the harden behavior of Ti-O modes above -80 °C marks the beginning of the region of fluctuating nanoregions. In a word, a more disordered lattice was presented in this material till room temperature accompanying with a macroscopic relaxor behavior, which promotes a high electrostrictive strain.

IV. Conclusion

Both dielectric and ferroelectric properties of BNT-BT-SBT systems were investigated. With the increase of SBT, the relaxor-like frequency dispersion became stronger near T_{R-T} with the shift of T_{R-T} to ambient temperature. A very high electrostrictive strain (~0.152%) with a high electrostrictive coefficient Q_{11} of 0.0297 m^4C^{-2} is observed at samples with x=0.3. Meanwhile, the Q_{11} maintains it at a high level from ambient temperature to 180 °C. The TEM and Raman spectroscopy revealed that the existence of nanodomains around room temperature at x=0.3 plays a key role in field-induced large electrostrictive strain.

ACKNOWLEDGEMENT

This work was supported by the National Natural Science Foundation (51172187), the SPDRF (20116102130002 and 20116102120016) and 111 Program (B08040) of MOE, the Xi'an Science and Technology Foundation (CX1261-2, CX1261-3 and CX12174), and the NPU Fundamental Research Foundation (NPU-FFR-JC201232) of China. J. Shi would like to thank Chinese Scholarship Council for financial support for working in the University of Leeds.

REFERENCES

[1]S.-E. Park and T. R. Shrout, "Ultrahigh Strain and Piezoelectric Behavior in Relaxor Based Ferroelectric Single Crystals," J. Appl. Phys., **82** [4] 1804-11 (1997).

[2] R. E. Newnham, Properties of Materials: Anisotropy, Symmetry, Structure; Ch. 12, pp. 87-100. Oxford University Press, Oxford, 2005.

[3]G. H. Haertling, "Ferroelectric Ceramics: History and Technology," J. Am. Ceram. Soc., **82** [4] 797-818 (1999).

[4]L. Bellaiche and D. Vanderbilt, "Intrinsic Piezoelectric Response in Perovskite Alloys: PMN-PT versus PZT," Phys. Rev. Lett., **83** [7] 1347-50 (1999).

[5]D. E. Cox, B. Noheda, G. Shirane, Y. Uesu, K. Fujishiro, and Y. Yamada, "Universal Phase Diagram for High-Piezoelectric Perovskite Systems," Appl. Phys. Lett., **79** [3] 400-2 (2001).

[6]E. M. Sabolsky, S. Trolier-McKinstry, and G. L. Messing, "Dielectric and Piezoelectric Properties of ⟨001⟩ Fiber-textured $0.675Pb(Mg_{1/3}Nb_{2/3})O_3$–$0.325PbTiO_3$ Ceramics," J. Appl. Phys., **93** [7] 4072-80 (2003).

[7]N. Lei, M. Zhu, P. Yang, L. Wang, L. Wang, Y. Hou, and H. Yan, "Effect of Lattice Occupation Behavior of Li^+ Cations on Microstructure and Electrical Properties of $(Bi_{1/2}Na_{1/2})TiO_3$-based Lead-free Piezoceramics," J. Appl. Phys., **109** [5] 054102, 6pp (2011).

[8]F. Gao, X. Dong, C. Mao, H. Zhang, F. Cao, and G. Wang, "Poling Temperature Tuned Electric-Field-Induced Ferroelectric to Antiferroelectric Phase Transition in $0.89Bi_{0.5}Na_{0.5}TiO_3$-$0.06BaTiO_3$-$0.05K_{0.5}Na_{0.5}NbO_3$ Ceramics," J. Appl. Phys., **110** [9] 094109, 4pp (2011).

[9]H. Simons, J. Glaum, J. E. Daniels, A. J. Studer, A. Liess, J. Rödel, and M. Hoffman, "Domain Fragmentation During Cyclic Fatigue in 94%$(Bi_{1/2}Na_{1/2})TiO_3$-6%$BaTiO_3$," J. Appl. Phys., **112** [4] 044101, 5pp (2012).

[10]J. Yao, N. Monsegue, M. Murayama, W. Leng, W. T. Reynolds, Q. Zhang, H. Luo, J. Li, W. Ge, and D. Viehland, "Role of Coexisting Tetragonal Regions in the Rhombohedral Phase of $Na_{0.5}Bi_{0.5}TiO_3$-xat.%$BaTiO_3$ Crystals on Enhanced Piezoelectric Properties on Approaching the Morphotropic Phase Boundary," Appl. Phys. Lett., **100** [1] 012901, 4pp (2012).

[11]R. Dittmer, W. Jo, J. Rödel, S. Kalinin, and N. Balke, "Nanoscale Insight Into Lead-Free BNT-BT-xKNN," Adv. Funct. Mater., **22** [20] 4208-15 (2012).

[12]R. Dittmer, E.-M. Anton, W. Jo, H. Simons, J. E. Daniels, M. Hoffman, J. Pokorny, I. M. Reaney, J. Rödel, and D. Damjanovic, "A High-Temperature-Capacitor Dielectric Based on $K_{0.5}Na_{0.5}NbO_3$-Modified $Bi_{1/2}Na_{1/2}TiO_3$-$Bi_{1/2}K_{1/2}TiO_3$," J. Am. Ceram. Soc., **95** [11] 3519-24 (2012).

[13]W. Jo, T. Granzow, E. Aulbach, J. Rödel, and D. Damjanovic, "Origin of the Large Strain Response in $(K_{0.5}Na_{0.5})NbO_3$-modified $(Bi_{0.5}Na_{0.5})TiO_3$–$BaTiO_3$ Lead-free Piezoceramics," J. Appl. Phys., **105** [9] 094102, 5pp (2009).

[14]E. Aksel, J. S. Forrester, B. Kowalski, M. Deluca, D. Damjanovic, and J. L. Jones, "Structure and Properties of Fe-modified $Na_{0.5}Bi_{0.5}TiO_3$ at Ambient and Elevated Temperature," Phys. Rev. B, **85** [2] 024121, 11pp (2012).

[15]C. Ma, X. Tan, E. Dul'kin, and M. Roth, "Domain Structure-dielectric Property Relationship in Lead-free $(1-x)(Bi_{1/2}Na_{1/2})TiO_3$-$xBaTiO_3$ Ceramics," J. Appl. Phys., **108** [10] 104105, 8pp (2010).

[16]D. Schütz, M. Deluca, W. Krauss, A. Feteira, T. Jackson, and K. Reichmann, "Lone-pair-induced Covalency as the Cause of Temperature- and Field-induced Instabilities in Bismuth Sodium Titanate," Adv. Funct. Mater., **22** [11] 2285-94 (2012).

[17]C. Ang and Z. Yu, "High, Purely Electrostrictive Strain in Lead-Free Dielectrics," Adv. Mater., **18** [1] 103-6 (2006).

[18]S.-T. Zhang, A. B. Kounga, W. Jo, C. Jamin, K. Seifert, T. Granzow, J. Rödel, and D. Damjanovic, "High-Strain Lead-free Antiferroelectric Electrostrictors," Adv. Mater., **21** [46] 4716-20 (2009).

[19]S.-T. Zhang, F. Yan, B. Yang, and W. Cao, "Phase diagram and electrostrictive properties of $Bi_{0.5}Na_{0.5}TiO_3$–$BaTiO_3$–$K_{0.5}Na_{0.5}NbO_3$ ceramics," Appl. Phys. Lett., **97** [12] 122901, 3pp (2010).

[20]V. D. N. Tran, H.-S. Han, C.-H. Yoon, J.-S. Lee, W. Jo, and J. Rödel, "Lead-free Electrostrictive Bismuth Perovskite Ceramics with Thermally Stable Field-induced Strains," Mater. Lett., **65** [17-18] 2607-9 (2011).

[21]C. Ang and Z. Yu, "Dielectric and ferroelectric properties in (Sr, Ni, Na)TiO_3 Solid Solutions," J. Appl. Phys., **107** [11] 114106, 5pp (2010).

[22]C. Ang and Z. Yu, "High remnant polarization in $(Sr_{0.7}Bi_{0.2})TiO_3$-$(Na_{0.5}Bi_{0.5})TiO_3$ solid solutions," Appl. Phys. Lett., **95** [23] 232908, 3pp (2009).

[23]K. Uchino, "Electrostrictive Effects in Antiferroelectric Perovskites," J. Appl. Phys., **52** [3] 1455-9 (1981).

[24]A. Furuta, "Dynamic Observation of Crack Propagation in Piezoelectric Multilayer Actuators," J. Am. Ceram. Soc., **76** [6] 1615-7 (1993).

[25]W. Jo, S. Schaab, E. Sapper, L. A. Schmitt, H.-J. Kleebe, A. J. Bell, and J. Rödel," On the phase identity and its thermal evolution of lead free $(Bi_{1/2}Na_{1/2})TiO_3$-6 mol% $BaTiO_3$," J. Appl. Phys., 110[7] 074106, 9pp (2011).

[26]R. Dittmer, W. Jo, J. Daniels, S. Schaab and J. Rödel, "Relaxor Characteristics of Morphotropic Phase Boundary $(Bi_{1/2}Na_{1/2})TiO_3$-$(Bi_{1/2}K_{1/2})TiO_3$ Modified with $Bi(Zn_{1/2}Ti_{1/2})O_3$," J. Am. Ceram. Soc., **94** [12] 4283-90 (2011).

[27]R. Dittmer, W. Jo, D. Damjanovic, and J. Rödel, "Lead-free High-Temperature Dielectrics with Wide Operational Range," J. Appl. Phys., **109** [3] 034107, 5pp (2011).

[28]M. Davis, D. Damjanovic, and N. Setter, "Electric-field-, Temperature-, and Stress-Induced Phase Transitions in Relaxor Ferroelectric Single Crystals," Phy. Rev. B, **73** [1] 014115, 16pp (2006).

[29]J. Yao, W. Ge, L. Yan, W. T. Reynolds, J. Li, D. Viehland, D. A. Kiselev, A. L. Kholkin, Q. Zhang, and H. Luo, "The influence of Mn substitution on the local structure of $Na_{0.5}Bi_{0.5}TiO_3$ Crystals: Increased Ferroelectric Ordering and Coexisting Octahedral Tilts," J. Appl. Phys., **111** [6] 064109, 6pp (2012).

[30]V. Dorcet, G. Trolliard, and P. Boullay, "Reinvestigation of Phase Transitions in $Na_{0.5}Bi_{0.5}TiO_3$ by TEM. Part I: First Order Rhombohedral to Orthorhombic Phase Transition," Chem. Mater., **20** [15] 5061-73 (2008).

[31]G. Trolliard and V. Dorcet, "Reinvestigation of Phase Transitions in $Na_{0.5}Bi_{0.5}TiO_3$ by TEM. Part II: Second Order Orthorhombic to Tetragonal Phase Transition," Chem. Mater., **20** [15] 5074-82 (2008).

[32]C. W. Tai and Y. Lereah, "Nanoscale Oxygen Octahedral Tilting in $0.90(Bi_{1/2}Na_{1/2})TiO_3$–$0.05(Bi_{1/2}K_{1/2})TiO_3$–$0.05BaTiO_3$ Lead-Free Perovskite Piezoelectric Ceramics," Appl. Phys. Lett., **95** [6] 062901, 3pp (2009).

[33]Y. Guo, M. Gu, H. Luo, Y. Liu, and R. L. Withers, "Composition-induced Antiferroelectric Phase and Giant Strain in Lead-free $(Na_y,Bi_z)Ti_{1-x}O_{3(1-x)}$-$xBaTiO_3$ Ceramics," Phys. Rev. B, **83** [5] 054118, 7pp (2011).

[34]C. J. Stringer and C. A. Randall, "In situ TEM Investigations of the High-Temperature Relaxor Ferroelectric $BiScO_3$-$Pb(Mg_{1/3}Nb_{2/3})O_3$-$PbTiO_3$Ternary Solid Solution," J. Am. Ceram. Soc., **90** [6] 1802-07 (2007).

[35]B. Wylie-van Eerd, D. Damjanovic, N. Klein, N. Setter, and J. Trodahl, "Structural Complexity of $(Na_{0.5}Bi_{0.5})TiO_3$-$BaTiO_3$ as Revealed by Raman Spectroscopy," Phys. Rev. B, **82** [10] 104112, 7pp (2010).

[36]D. Rout, K.-S. Moon, V. S. Rao, and S.-J. L. Kang, "Study of the Morphotropic Phase Boundry in the Lead-Free $Na_{1/2}Bi_{1/2}TiO_3$-$BaTiO_3$ System by Raman Spectroscopy," J. Ceram. Soc. Jpn., **117** [7] 797-800 (2009).

[37]L. Luo, W. Ge, J. Li, D. Viehland, C. Farley, R. Bodnar, Q. Zhang, and H. Luo, "Raman Spectroscopic Study of $Na_{1/2}Bi_{1/2}TiO_3$-x%$BaTiO_3$ Single Crystals as a Function of Temperature and Composition," J. Appl. Phys., **109** [11] 113507, 6pp (2011).

[38]J. Suchanicz, I. Jankowska-Sumara, and T. V. Kruzina, "Raman and Infrared Spectroscopy of $Na_{0.5}Bi_{0.5}$TiO3-$BaTiO_3$ Ceramics," J. Electroceram., **27** [2] 45-50 (2011).

[39]J. Kreisel, A. M. Glazer, G. Jones, P. A. Thoma, L. Abello, and G. Lucazeau, "An X-Ray Diffraction and Raman Spectroscopy Investigation of A-site Substituted Perovskite Compounds," J. Phys.: Condens. Matter, **12** 3267-80 (2000).

[40]D. Rout, K.-S. Moon, S.-J. L. Kang, and I. W. Kim, "Dielectric and Raman Scattering Studies of Phase Transitions in the $(100-x)Na_{0.5}Bi_{0.5}TiO_3–xSrTiO_3$ System," J. Appl. Phys., **108** [8] 084102, 7pp (2010).

[41]F. Wang, M. Xu, Y. Tang, T. Wang, W. Shi, C. M. Leung, and J. Rödel, "Large Strain Response in the Ternary $Bi_{0.5}Na_{0.5}TiO_3$-$BaTiO_3$-$SrTiO_3$ Solid Solutions," J. Am. Ceram. Soc., **95** [6] 1955-59 (2012).

[42]A. Slodczyk, P. Colomban, and M. Pham-Thi, "Role of the TiO_6 Octahedra on the Ferroelectric and Piezoelectric Behaviour of the Poled $PbMg_{1/3}Nb_{2/3}O_{3-x}PbTiO_3$(PMN-PT) Single Crystal and Textured Ceramic," J. Phys. Chem. Solids, **69** [10] 2503-13 (2008).

Figure captions

FIG. 1. X-ray diffraction patterns of BNT-BT-xSBT with x=0-0.5, the inset shows the SEM images of the surface of BNT-BT-0.3SBT.

FIG. 2. (a) Polarization (P) versus electric field (E), and (b) Strain (S) versus electric field (E) at 1 Hz for the samples with x=0, 0.1, 0.3 and 0.5 at ambient temperature. (c) Strain (S) versus the square polarization (P^2) for the samples with x=0.1 and 0.3 at ~80 kV/cm at ambient temperature.

FIG. 3. Temperature dependence of the polarization (P) versus electric field (E) of different temperatures at ~60 kV/cm for x=0.3. The insets show the strain (S), electrostrictive coefficient Q_{11} at ~60 kV/cm and maximum polarization P_{max} of different temperatures.

FIG. 4. Temperature dependence of the relative dielectric permittivity (ε') and loss tangent ($\tan\delta$) for the BNT-BT-xSBT at different frequencies. The inset of x=0.3 shows $\Delta\varepsilon'$ (ε'_{1kHz}-ε'_{100kHz}) of samples with x=0, 0.1, 0.3 and 0.5 at ambient temperature.

FIG. 5. (a) Bright field TEM image, which shows grainy morphology ferroelectric domains for x=0.1. (b), (c), SAED patterns of x=0.1 along the [100] and [110] zone axis. (d) Bright field TEM image, which shows nano-sized ferroelectric domains for x=0.3, the inset shows the larger version of nanodomains of x=0.3. (e), (f), SAED patterns of x=0.3 along the [100] and [110] zone axis, where 1/2 ooo superlattice reflections are marked by arrows, 1/2 ooe ones by rings.

FIG. 6. (a) Ambient temperature Raman spectroscopy for samples with x=0, 0.1 and 0.3, with an inset showing spectral deconvolution to Lorentzian function for the sample with x=0.3. (b) Temperature dependent Raman spectroscopy from -160 ^{o}C-0 ^{o}C. The inset shows the temperature dependence of the position of both the Bi-O and Ti-O modes.

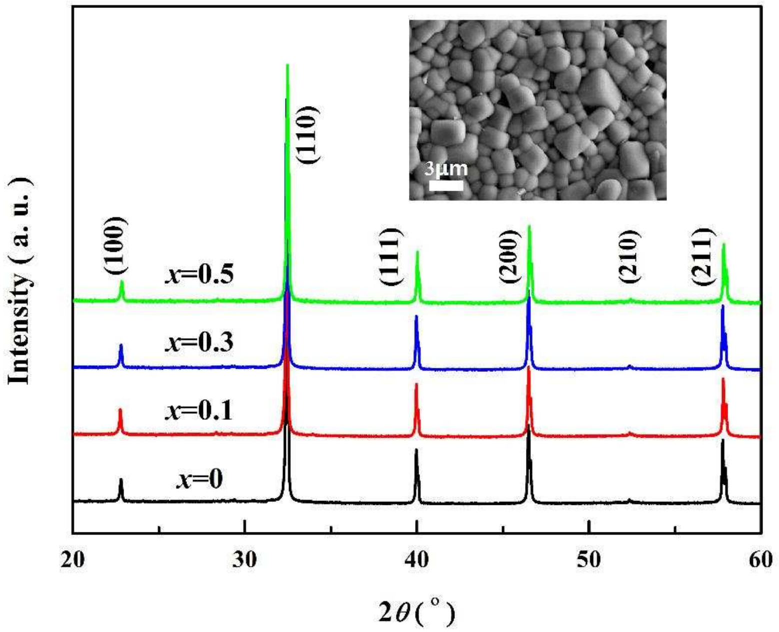
Intensity (a. u.)
2θ (°)
20
30
40
50
60
x=0.5
x=0.3
x=0.1
x=0
(100)
(110)
(111)
(200)
(210)
(211)
3μm

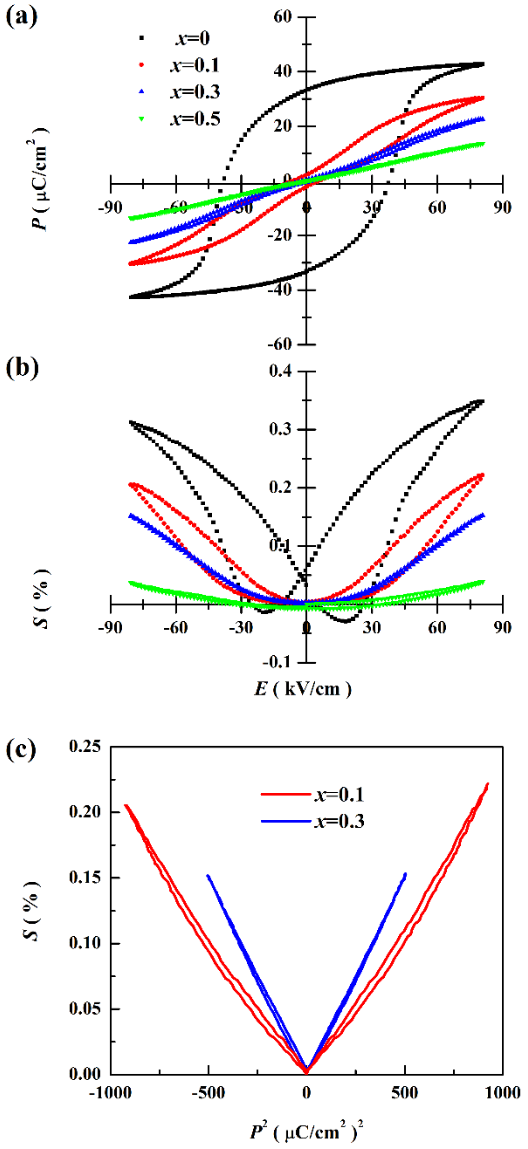
(a)
x=0
x=0.1
x=0.3
x=0.5
P (μC/cm^2)
60
40
20
0
-20
-40
-60
-90
-60
-30
0
30
60
90
(b)
S (%)
0.4
0.3
0.2
0.1
-0.1
-90
-60
-30
0
30
60
90
E (kV/cm)
(c)
x=0.1
x=0.3
S (%)
0.25
0.20
0.15
0.10
0.05
0.00
-1000
-500
0
500
1000
P^2 (μC/cm^2)^2

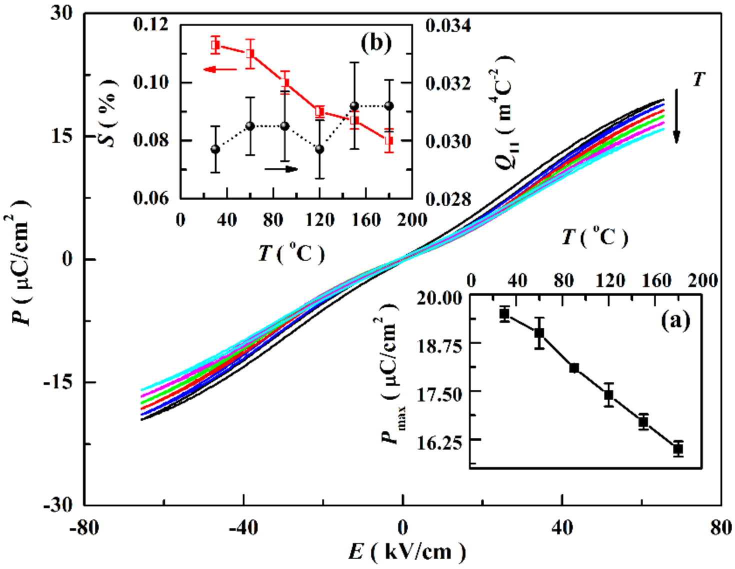
30
15
0
-15
-30
-80
-40
0
40
80
P (μC/cm2)
E (kV/cm)
T
(b)
0.12
0.10
0.08
0.06
0.034
0.032
0.030
0.028
0
40
80
120
160
200
S (%)
Q11 (m4C-2)
T (°C)
T (°C)
0
40
80
120
160
200
(a)
20.00
18.75
17.50
16.25
Pmax (μC/cm2)

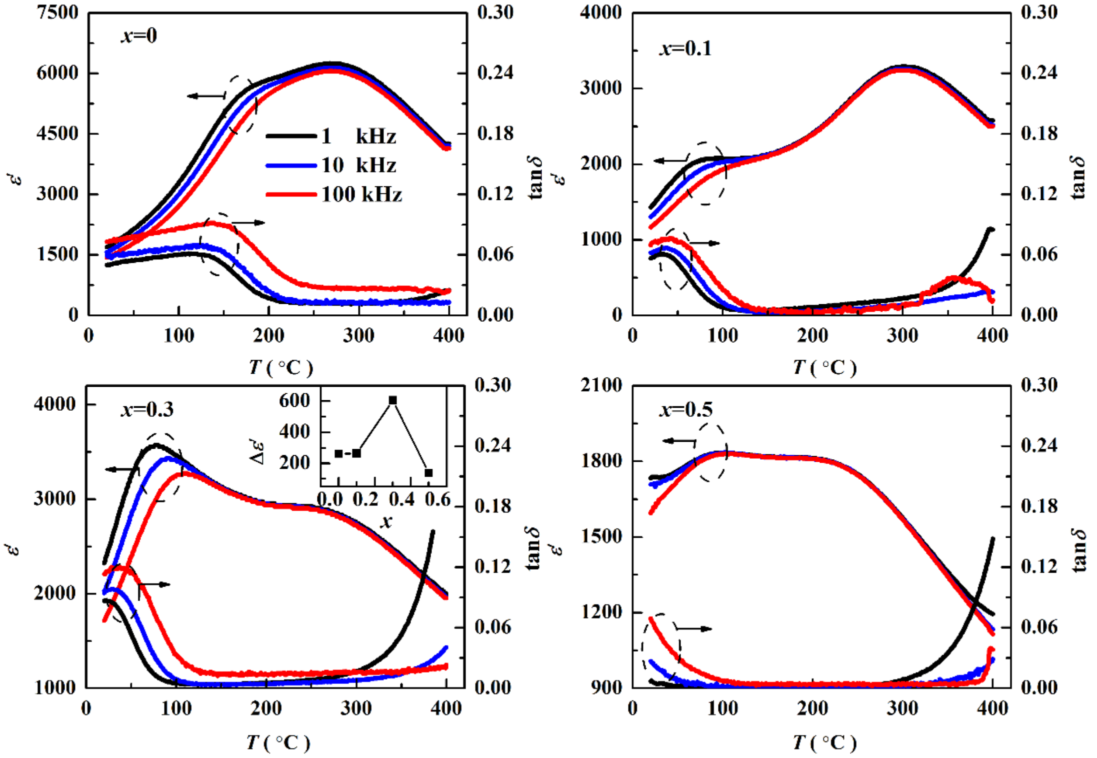

x=0
x=0.1
x=0.3
x=0.5
1 kHz
10 kHz
100 kHz
ε′
tanδ
T (°C)
Δε′
x
0
100
200
300
400
7500
6000
4500
3000
1500
4000
2000
1000
2100
1800
1500
1200
900
600
400
200
0.0
0.2
0.4
0.6
0.00
0.06
0.12
0.18
0.24
0.30

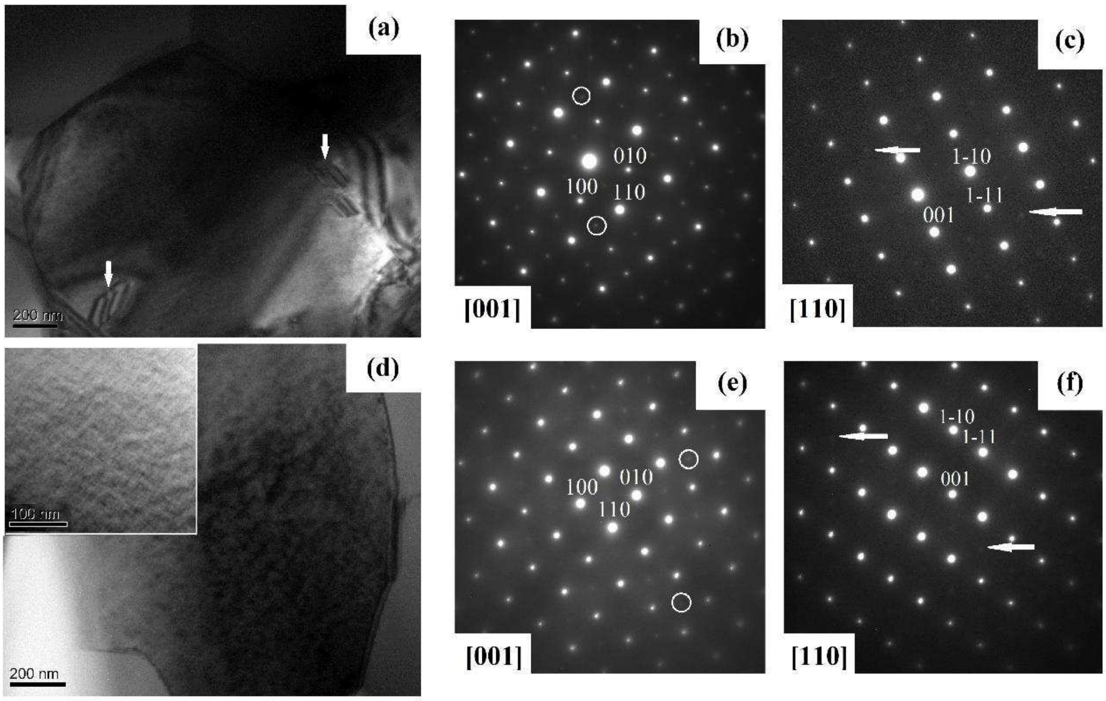
(a)
200 nm
(b)
010
100
110
[001]
(c)
1-10
1-11
001
[110]
(d)
100 nm
200 nm
(e)
100
010
110
[001]
(f)
1-10
1-11
001
[110]

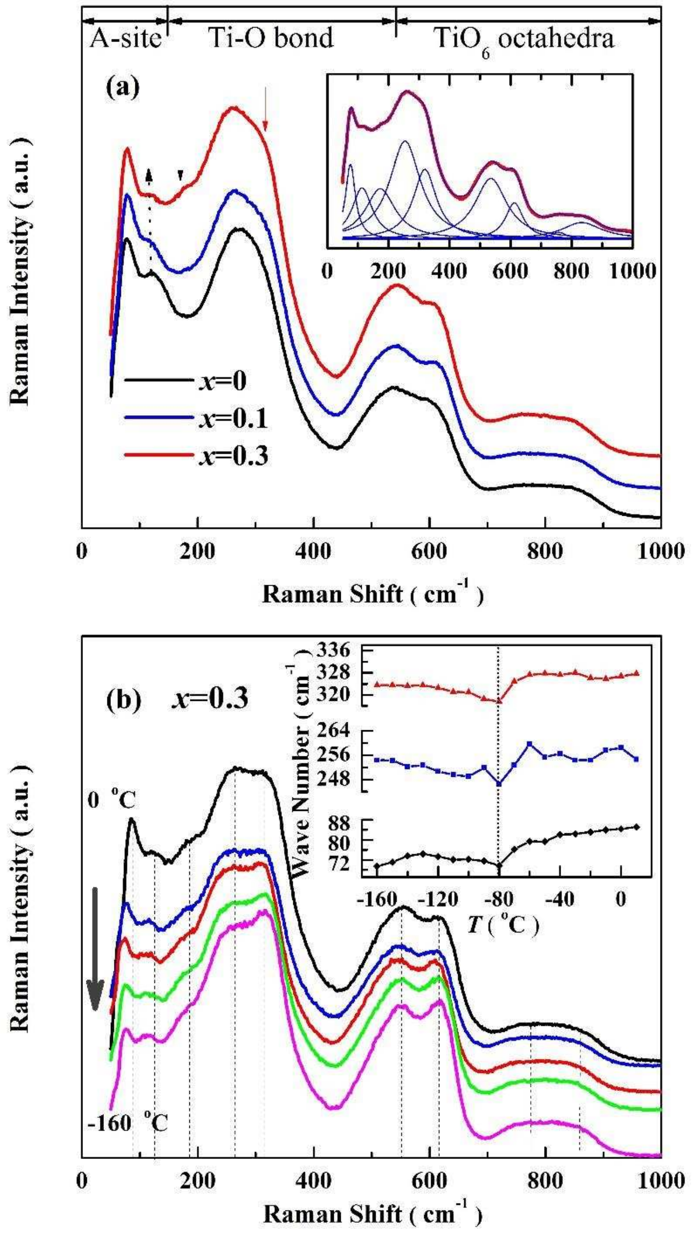
A-site
Ti-O bond
TiO$_6$ octahedra
(a)
Raman Intensity (a.u.)
x=0
x=0.1
x=0.3
0
200
400
600
800
1000
Raman Shift (cm^{-1})
(b) x=0.3
0 °C
-160 °C
Wave Number (cm^{-1})
336
328
320
264
256
248
88
80
72
-160
-120
-80
-40
0
T (°C)